

Wiseman-Milburn Control for the Lipkin-Meshkov-Glick Model

Sven Zimmermann,¹ Wassilij Kopylov,^{1,*} and Gernot Schaller¹

¹*Institut für Theoretische Physik, Technische Universität Berlin, D-10623 Berlin, Germany*
(Dated: June 14, 2021)

We apply a measurement-based closed-loop control scheme to the dissipative Lipkin-Meshkov-Glick model. Specifically, we use the Wiseman-Milburn feedback master equation to control its quantum phase transition. For the steady state properties of the Lipkin-Meshkov-Glick system under feedback we show that the considered control scheme changes the critical point of the phase transition. Finite-size corrections blur these signatures in operator expectation values but entanglement measures such as concurrence can be used to locate the transition point more precisely. We find that with feedback, the position of the critical point can be shifted to smaller spin-spin interactions, which is potentially useful for setups with limited control on these.

I. INTRODUCTION

Quantum criticalities arising in different types of phase transitions such as lasing transitions or quantum phase transitions (QPTs) belong to classical but still modern and important research. This is particularly true in non-equilibrium setups [1–4]. Whereas in case of the laser transition the coherence is shared by the photons that induce a macroscopic occupation of a light mode and the inverted atoms serve just as a battery, in case of the Hepp-Lieb quantum phase transition the collective coupling between different atoms is the key to the light flash.

The prominent examples for collective critical models are the Dicke and Lipkin-Meshkov-Glick (LMG) models, where N collectively coupled excited atoms in non-equilibrium produce a light flash with N^2 intensity during their decay [5, 6]. Collectivity is at the heart of such systems, and criticality is even present without any coupling to an environment already in the closed forms of such models. These are well studied and their transitions are known as the Hepp-Lieb QPT from a normal to a superradiant or symmetry-broken state, where the phases are separated by a closing energy gap between the two lowest energy states. Additionally, the quantum fluctuations diverge at the phase transition [7–13].

In the last decades, the fate of QPTs and their impact on the emission properties have been studied in open and non-equilibrium set-ups far from thermal equilibrium [14–19].

Due to the high degree of parameter control in already existing experimental cold-atom realizations of such models [20, 21] new ideas have come up, particularly to study the effect of control loops on QPTs.

In general, one can divide control in two kinds, closed-loop (feedback) control and open control. Here, the difference is that closed-loop control in some way feeds information on a system state back into the system. In quantum (classical) mechanics, feedback control is usually further subdivided into coherent (autonomous) and

measurement-based (external) feedback control. Many investigations have been performed by applying such schemes to quantum systems. For example, using an open control by periodically driving one parameter, new quantum phases could be created, entanglement modified or the emission properties changed [22–24]. Similar and other effects like modification of the non-equilibrium steady state properties are possible with closed control loops, too. This is also the case when an additional time-delay term is taken into account [25–31].

Wiseman-Milburn feedback is one special example of a measurement-based control loop. Here, the idea is to continuously monitor the reservoir coupled to the system and to perform a quantum operation on the system whenever a special event like a photon emission is observed [32]. In certain limits, such control operations appear on the level of the master equation as a simple unitary modification of the jump term [33]. Wiseman-Milburn feedback can for example be used to stabilize pure states of different systems even in non-equilibrium [34–36], which has been experimentally demonstrated [37, 38]. Moreover, the impact of such schemes on the first and second laws of thermodynamics [39] has been studied.

In this paper, our main idea is to apply Wiseman-Milburn feedback to the dissipative LMG system, where dissipation effectively corresponds to photon emission [18, 40]. Experimentally, the scheme requires to apply after each photon emission a unitary kick along one of the three collective angular momentum axes. Formally, this corresponds to a rotation of the jump part in the master equation around the chosen axis. The rotation angle is then the feedback control parameter. We will concentrate on the non-equilibrium steady state of the finite-size LMG system in presence of the considered feedback action. In particular, we show for finite-size LMG models that in presence of feedback the non-trivial steady state expectation values of the spin operators can be reached for a smaller spin-spin coupling. This may be useful as an additional control knob in experiments investigating critical behaviour. We argue that in the thermodynamic limit, the dissipative QPT, which in absence of feedback can be observed already with mean-field methods, becomes shifted toward a smaller spin-spin coupling

* kopylov@itp.tu-berlin.de

as well. Furthermore, we show that such a shift is visible in the entanglement properties of the LMG system with feedback, too, which we will calculate in the dissipative context using the concurrence [41, 42].

Our paper is structured as follows. In sections II A and II B we will review the major properties of the closed and open LMG system, which are important to understand the feedback-induced effects. In section II C we will introduce the feedback scheme. In section III we will show how such a control scheme changes the steady state. We will investigate the properties of the spin expectation values and the concurrence. Finally, in section IV we will conclude and sum up the results.

II. MODEL

A. Closed System

The fully anisotropic Lipkin-Meshkov-Glick (LMG) Hamiltonian is given by [43]

$$H_{LMG} = -hJ_z - \frac{\gamma_x}{N} J_x^2, \quad (1)$$

where γ_x is the interaction between each pair of the N system spins and h is the strength of the magnetic field in z direction. Due to the all-to-all coupling, the collective angular momentum operators can be used

$$J_\eta = \frac{1}{2} \sum_{n=1}^N \sigma_\eta^{(n)}, \quad \eta \in \{x, y, z\}, \quad (2)$$

$$J_\pm = J_x \pm iJ_y,$$

where $\sigma_\eta^{(n)}$ are the common Pauli matrices of the n -th spin.

The collective angular momentum operators mirror the properties of the single spin angular momentum $[J_x, J_y] = iJ_z$, and their action on the eigenvectors $|j, m\rangle$ is given by

$$J^2 |j, m\rangle = j(j+1) |j, m\rangle, \quad (3)$$

$$J_z |j, m\rangle = m |j, m\rangle,$$

where $j \in \{0, \dots, N/2\}$ is the total angular momentum quantum number which can only assume half-integer or integer values, and the projection m of the angular momentum to the z -axis bounds the second quantum number by $m \in \{-j, j\}$. The ladder operators act as follows

$$J_\pm |j, m\rangle = \sqrt{j(j+1) - m(m \pm 1)} |j, m \pm 1\rangle. \quad (4)$$

We observe that the angular momentum $J^2 = J_x^2 + J_y^2 + J_z^2 = \frac{1}{2} [J_-, J_+]_+ + J_z^2$ is conserved in case of the LMG system, as it commutes with the systems Hamiltonian (1). This follows directly from $[J^2, J_\eta] = 0$. Therefore, the Hilbert space for different angular momenta j

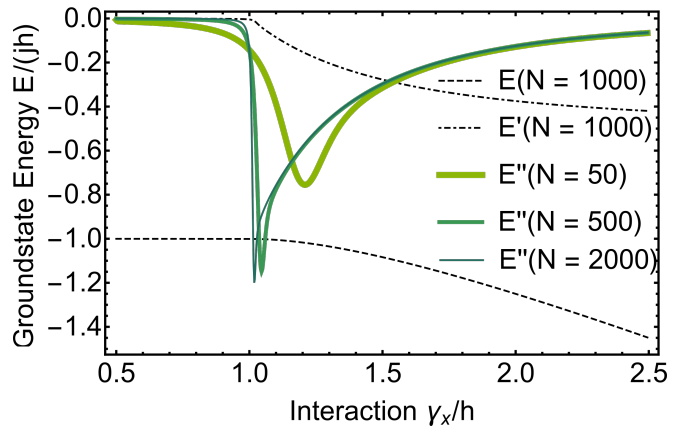


FIG. 1. Plot of the LMG ground state energy density and its first two derivatives for different N . For a larger N , the minimum of the second derivative is further shifted to $\gamma_x/h = 1$ and becomes sharper, see green solid lines with decreasing thickness. In the thermodynamic limit $N \rightarrow \infty$, the second derivative is not continuous any more and thus the ground state is not analytic at $\gamma_x = h$ which indicates that the phase transition is of second order.

decouples. Throughout this paper, we will restrict ourselves to the part of the Hilbert space with the maximum angular momentum

$$j = \frac{N}{2}, \quad (5)$$

as this subspace contains the ground and the first excited state. Furthermore, this subspace can be specifically realized in the experimental setups [13, 21, 44].

Another conserved quantity in the closed LMG model is the parity operator [45, 46], and we can define projectors onto the subspaces with positive or negative parity via

$$P_\pm = \frac{1}{2} [1 \pm \exp(i\pi J_z) \exp(i\pi N/2)]. \quad (6)$$

One of the intriguing properties of the LMG model is the appearance of a quantum phase transition (QPT) in the thermodynamic limit $N \rightarrow \infty$ at a critical value of the coupling $\gamma_x/h = 1$ [13, 47–49]. Fig. 1 shows the ground state energy per atom pair (dashed line) and its first two derivatives. Also the second derivative E'' with respect to γ_x is shown for different spin numbers N (solid green curves with different thickness), and it becomes discontinuous in the thermodynamic limit at $\gamma_x/h = 1$, which indicates the appearance of the second order QPT in the ground state energy per atom pair.

However, the excited part of the LMG spectrum has an additional phase transition – the excited states quantum phase transition (ESQPT) [44, 50–54]. It is visible in Fig. 2, which shows the spectrum of the LMG model for $j = N/2$ as a function of γ_x for $N = 50$. The signature of

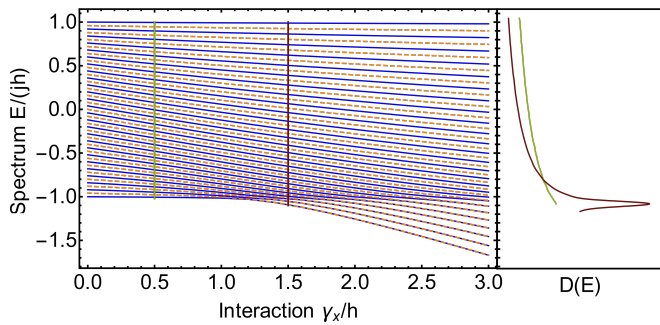


FIG. 2. (left) Energy spectrum of the LMG Hamiltonian for $N = 50$ versus the interaction γ_x . The colors indicate the parity of the state: blue (solid) for positive and orange (dashed) for negative parity. The QPT precursor is visible around $\gamma_x \approx 1.3h$ due to finite size effects. For $N \rightarrow \infty$ this will shift to $\gamma_x = h$ (compare with Fig. 1). Additionally, the higher density of states around $E = -jh$ signals the ESQPT. (right) The density of states versus the energy at $\gamma_x = 0.5h$ (green) and $\gamma_x = 1.5h$ (red) for $N = 1000$ as indicated in the left panel. The peak is visible only for $\gamma_x > h$ and corresponds to the ESQPT.

the ESQPT is the non-analyticity in the density of states

$$D(E) = \frac{1}{V} \sum_{i=1}^{N+1} \delta(E - \epsilon_i), \quad (7)$$

which is visible in the symmetry-broken phase. Here, V is a normalization constant and ϵ_i is the i th eigen-energy of the system. Although strictly speaking the non-analyticity appears only in the thermodynamic limit, in case of the LMG model it is already visible in Fig. 2(left) as a dense region in the spectrum around $E/(jh) = -1$. The right panel of Fig. 2 shows the density of states numerically determined for $N = 1000$ along the green and brown vertical lines indicated in the left panel. For $\gamma_x/h > 1$ (brown curve) the density of states has a logarithmic divergence, which marks the ESQPT [43, 44, 51, 55, 56].

B. Open System

The dynamics of an open LMG system can be described in the master equation formalism according to Ref. [18] via

$$\dot{\rho} = -i[H_{\text{LMG}}, \rho] + \frac{\kappa}{N} \mathcal{D}[J_+] \rho. \quad (8)$$

Here, $\kappa \geq 0$ quantifies the strength of dissipation, which as a super-operator acts as

$$\mathcal{D}[J_+] \rho = \frac{1}{2} (2J_+ \rho J_- - J_- J_+ \rho - \rho J_- J_+). \quad (9)$$

For $h > 0$ and $\gamma_x = 0$ we see that this dissipator has the pure state $|j, +j\rangle$ as a stationary state, which is the

ground state of H_{LMG} for $\gamma_x = 0$ and $h > 0$. In general, the steady state will be a mixed non-equilibrium state.

The master equation can be rewritten in terms of the super operators [57, 58]

$$\dot{\rho} = \mathcal{L}\rho = \mathcal{L}_0\rho + \mathcal{J}\rho, \quad (10)$$

with the free Liouvillian $\mathcal{L}_0\rho = -i(H_{\text{eff}}\rho - \rho H_{\text{eff}}^\dagger)$, which describes the system evolution without jumps, and the jump superoperator $\mathcal{J}\rho = \frac{\kappa}{N} J_+ \rho J_-$. Note that here, H_{eff} is an effective non-hermitian Hamiltonian [57, 59, 60]

$$H_{\text{eff}} = H_{\text{LMG}} - \frac{i}{2} \frac{\kappa}{N} J_- J_+. \quad (11)$$

The total angular momentum J is conserved even in presence of dissipation ($\kappa > 0$), but not the parity. Due to the presence of the all-to-all coupling, the dynamics of the observables governed by the master equation (8) can be very well described using only the first-order moments in mean-field approximation $\langle J_\eta \cdot J'_\eta \rangle \approx \langle J_\eta \rangle \cdot \langle J'_\eta \rangle$ [40, 42, 54]. The approximation yields up to four different steady-state solutions.

In presence of dissipation, the critical point is now defined by the stability exchange of those steady states at

$$\gamma_x^{\text{cr}} = h + \frac{\kappa^2}{4h}. \quad (12)$$

Fig. 3 summarizes the steady state properties governed by the mean-field equations. The QPT is in this picture represented by a bifurcation, visible in the spin expectation values. While in the normal phase for $\gamma_x < \gamma_x^{\text{cr}}$ there is one stable (solid) and one unstable (not shown) fixed point, in the symmetry broken phase for $\gamma_x > \gamma_x^{\text{cr}}$ the stable fixed point of the normal phase becomes unstable (dashed lines), and two new stable fixed points appear (solid curves with different thickness). Thus at γ_x^{cr} the solution properties change drastically, the stable solution (solid) of the normal phase becomes unstable (dashed) and a new stable solution is created via a pitchfork bifurcation (solid). More details are presented in App. IV.

C. Controlled System

In this section, we extend the dynamics of the open LMG system by the Wiseman-Milburn control operation [32]. The idea is to apply an instantaneous unitary control operation \mathcal{C} on the density matrix after each jump \mathcal{J}

$$\mathcal{C}\rho = U_C \rho U_C^\dagger. \quad (13)$$

Such a measurement-based feedback can be described on the master equation level, where Eq. (10) is altered to [32, 35, 39],

$$\dot{\rho} = \mathcal{L}\rho = \mathcal{L}_0\rho + \mathcal{C}\mathcal{J}\rho. \quad (14)$$

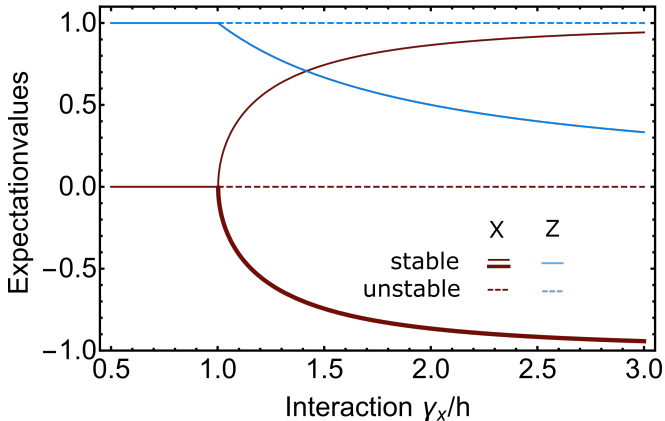


FIG. 3. Plot of the mean-field stationary large-spin expectation values $X = \langle J_x \rangle_{t \rightarrow \infty} / j$, $Z = \langle J_z \rangle_{t \rightarrow \infty} / j$ versus spin-spin interaction strength γ_x in the thermodynamic limit for $\kappa/h = 0.05$. The stable trivial solution with $Z = 1$ (solid) becomes unstable at γ_x^{cr} from Eq. (12) (dashed). But two new stable solutions (distinguishable by X) are created by a pitchfork bifurcation for $\gamma_x > \gamma_x^{\text{cr}}$ (solid) with $Z < 1$.

We consider simple rotations conserving the total angular momentum

$$U_C = \exp \left[-\frac{i}{\sqrt{N}} (\theta_x J_x + \theta_y J_y + \theta_z J_z) \right], \quad (15)$$

where the θ_α are real control parameters and where we have introduced the factor \sqrt{N} to ensure for convergence of stationary expectation values in the thermodynamic limit.

In the following, we will always use either $\theta_x \neq 0$ or $\theta_z \neq 0$, as other combinations are either producing similar effects as rotation around x or z axis or could not improve them. Usually, the Wiseman-Milburn scheme can be used to stabilize the eigenstates of the effective non-hermitian Hamiltonian Eq. (11) [35, 36] by a rotation of the state after each jump to such an eigenstate. However, in our case this is not applicable, as higher-order terms like $J_\eta^n J_{\eta'}^{n'}$ would have to be used to achieve this. Despite this restriction, we will show in the next section that even a single J_x or J_z rotation can dramatically change the systems steady state, modify its entanglement and shift the point of the phase transition.

Before proceeding to the results, we note that a simple mean-field analysis is not applicable here. We found that in presence of feedback, the simple mean-field approximation violates the conservation of total angular momentum. Likewise, analysis of H_{eff} [60] cannot reveal any feedback-induced effect as H_{eff} is insensitive to it. Instead, the full feedback master equation Eq. (14) has to be solved numerically for its steady state, which is more demanding and restricts our study to the finite-size regime.

III. IMPACT ON THE STEADY STATE

In this section, we discuss the steady state properties of the LMG system under the jump-based feedback action for a finite number of atoms N . In practice, we numerically determine the stationary state of Eq. (14). Below, we first show how the typical observables like the spin expectation values are changed under the feedback and discuss their connection to the QPT. Later, we will investigate the systems entanglement.

A. Observables in the new steady state

We start our discussion by showing in Fig. 4 the $\langle J_z \rangle$ expectation values in the steady state of Eq. (14) as a function of the interaction strength γ_x and the control angle θ_x (left, for $\theta_y = \theta_z = 0$) or θ_z (right, for $\theta_x = \theta_y = 0$). Note the logarithmic scaling of the y-axis.

Our numerics shows that in presence of the considered feedback scheme for $\theta_x > 0$, the decay of the $\langle J_z \rangle$ expectation value is observed for smaller γ_x , see Fig. 4(left). The contour lines are shifted then toward the smaller γ_x values. For small θ_x values the shift is approximately linear, then for $1.5 < \log(\theta_x + 1) < 3$ the position of $\langle J_z \rangle$ values does not change much. For even larger θ_x values the deviation of $\langle J_z \rangle$ from its maximal value $j = N/2$ is again strongly shifted to the left. For $\log(\theta_x + 1) \rightarrow \log(\pi\sqrt{N} + 1) \approx 3.24$ this point shifts to $\gamma_x \rightarrow 0$.

We will elaborate this findings by comparing the behaviour for two fixed θ_x parameters. The $\langle J_z \rangle(\gamma_x)$ expectation values along the dashed ($\theta_x = 0$) and solid ($\theta_x = 2$) horizontal lines in Fig. 4(left) are shown in Fig. 5(top), see dashed and solid line for $N = 50$, respectively. In absence of feedback (dashed lines), the case is well studied [13, 61] and the expectation values may serve as a signature of the QPT. Indeed, for an increasing number of particles N the $J_z(\gamma_x)$ curves become more irregular around the critical point, see dotted blue lines marked by different symbols for three different values of N . The visibility of this signature is improved in the first derivative $\partial_{\gamma_x} J_z$ as a minimum, see Fig. 5(bottom), which becomes sharper with increasing N and finally becomes discontinuous in the thermodynamic limit $N \rightarrow \infty$ at $\gamma_x = \gamma_x^{\text{cr}} = h + \kappa^2/(2h)$ where the dissipative QPT occurs (this case is not shown in Fig. 5, see Fig. 3 instead).

Associating the critical point of the dissipative QPT with the $\langle J_z \rangle$ deviation from its maximum value means that the considered control scheme pushes the point of the dissipative QPT to a smaller critical value than in the $\theta = 0$ case. For $\theta_x = 2$ we demonstrate this behaviour by plotting $\langle J_z \rangle$ across the horizontal solid line in the contour plot, see the unmarked solid curve for $N = 50$ in Fig. 5 (top). The expectation value $\langle J_z \rangle$ remains first constant with the increasing coupling γ_x , then it starts to decrease. The value of γ_x , where the decrease takes place, is changed by the feedback in comparison to the

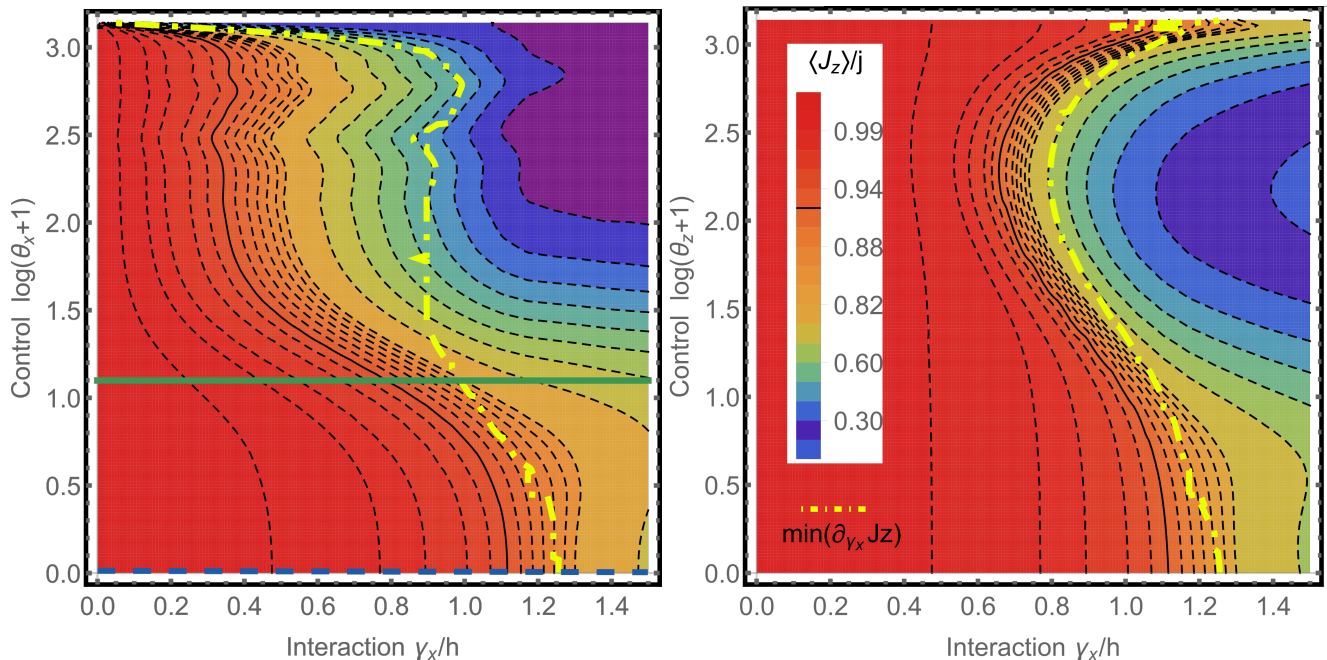


FIG. 4. The normalized expectation values $\langle J_z \rangle / j$ versus the interaction γ_x and the control angle θ_x (left) or θ_z (right) for $N = 50$ and $\kappa = 0.05h$. The solid contour line shows the $\langle J_z \rangle = 0.93$ -value where the finite-size QPT occurs in the $\theta = 0$ case. The dot-dashed line shows the position of the minimum of the derivative of $\langle J_z \rangle$ with respect to γ_x . Increasing the control parameter θ shifts the onset of the transition towards the smaller γ_x values, see the trend of the contour lines around the solid one. In case of the J_z control (right) this trend is reversed for higher θ_z values. However, the critical point can be determined only approximately due to the presence of finite-size effects. The $\langle J_z \rangle$ values and their derivatives along the horizontal dotted ($\theta_x = 0$) and solid lines ($\theta_x = 2$) in the left contour plot are shown in Fig. 4. Note the logarithmic scaling of the y-axis, thus the maximal θ_η value which we use is $\pi\sqrt{N} \approx 22$.

$\theta_x = 0$ case (dotted lines). The latter is especially visible in the derivative with respect to γ_x , see Fig. 5(bottom). That means, that the feedback forces the system to leave the usually stable solution – after passing the now θ_x -dependent critical γ_x value – with its maximal $\langle J_z \rangle$ value and to converge to another one, with $\langle J_z \rangle < 0$. The latter solution is typical for the symmetry broken phase of the uncontrolled LMG model. Additionally, for each curve, we show the finite-size scaling of the results by labelling the correspondent curve with open (filled) symbols for $N = 30(100)$. Besides the feedback-induced shift of the dissipative QPT which was discussed above, the calculation shows that larger N lead to a more discontinuous shape in the vicinity of the critical point as expected.

Due to finite size effects, the position of the shifted dissipative phase transition can only be determined approximately. The solid contour line in Fig. 4 shows the J_z value, at which the finite-size precursor of the QPT in absence of feedback takes place. In contrast, the thick dot-dashed line in Fig. 4 shows the position of the minimum of $\partial_{\gamma_x} J_z$ for different θ_x values. Obviously, these curves do not coincide. Changing the number of particles N , see Fig. 5(bottom), or analysing e.g. the $\langle J_x^2 \rangle$ value instead would lead to a considerable shift of the solid and dot-dashed lines in the phase diagram. The presence of the QPT in the Hamiltonian part leads to os-

cillations right from the minimum of the $\langle J_z \rangle$ derivative, see green lines in Fig. 5 (bottom). We checked that the beginning of the oscillations coincides with the minima of the $\partial_{\gamma_x} \langle J_x \rangle$ in case without feedback. As the calculation for much larger N becomes rather involved, we show in the next chapter that the use of concurrence allows to fix the position of the QPT for in presence of feedback much more precise.

In case of the active θ_z control, the feedback impact on the steady state properties of $\langle J_z \rangle$ is qualitatively similar, but the shift is much smaller. Both phases are always clearly separated and the smallest γ_x where the $\langle J_z \rangle$ starts to deviate from j is reached around $0.8h$ for $\theta_z = \frac{\pi}{2}\sqrt{N}$, see right part of Fig. 4.

B. Entanglement

Due to the presence of dissipation in our model, the stationary density matrix is not a pure state, and the entanglement cannot [62] be characterized by the common 'von Neumann entropy' $S(\sigma) = -\text{Tr} \sigma \ln \sigma$ of a reduced part of the system density matrix $\sigma = \text{Tr}_{\text{part}} \{\rho\}$ [63]. Instead, the Wootters concurrence has to be used, which in general is very hard to calculate [64]. However, it is possible to calculate it from the reduced density matrix

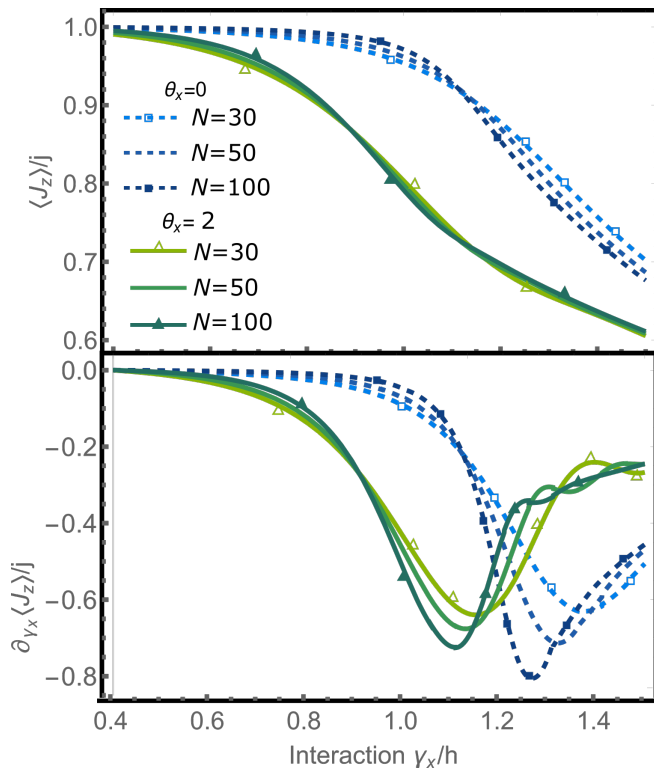


FIG. 5. The expectation values $\langle J_z \rangle$ (top) and the derivative $\partial_{\gamma_x} \langle J_z \rangle$ (bottom) over the interaction γ_x for $\theta_x = 0$ (blue dashed lines) and $\theta_x = 2$ (green solid lines) along the the horizontal lines in Fig. 4(left) for $N = 50$. Curves marked by open (closed) symbols additionally show the finite size effects for $N = 30(100)$. Increase of the control angle θ_x shifts the point where the $\langle J_z \rangle$ value starts to strongly deviate from its maximum value and shifts the position of the minimum in the derivative.

of two Qbits in an arbitrary basis [41]. The concurrence is bounded between zero and one and gives the amount of entanglement between two Qbits. In case of symmetric states – to which we constrain ourselves by considering the $j = N/2$ subspace only – it is possible to express the concurrence C_R using the large-spin observables [40, 65].

$$C_R = \begin{cases} 2 \max \left[0, \frac{|\langle J_+^2 \rangle|}{N} - \frac{\langle J_x^2 \rangle + \langle J_y^2 \rangle}{N} + \frac{1}{2} \right], & \frac{N^2 - 4\langle J_z^2 \rangle}{2N} < B, \\ 2 \max \left[0, \frac{N}{4} - \frac{\langle J_z^2 \rangle}{N} - S \right], & \frac{N^2 - 4\langle J_z^2 \rangle}{N} \geq B, \end{cases} \quad (16)$$

$$S = \frac{\sqrt{[N(N-2) + 4\langle J_z^2 \rangle]^2 - [4(N-1)\langle J_z \rangle]^2}}{4N},$$

$$B = S + \frac{|\langle J_+^2 \rangle|}{N}.$$

Concurrence has been widely studied in collective systems like LMG or Dicke models with and without dissipation [24, 40, 42, 63, 66–68]. Here we will use the modified steady state in presence of Wiseman-Milburn

feedback term to study the modification of the concurrence and compare it with the known cases.

The blue dashed lines in the inset of Fig. 6(left) show the concurrence of the open system $\kappa \neq 0$ without feedback $\theta_x = 0$ for three different N -values [40, 42]. Increasing γ_x , the concurrence C_R grows in the normal phase, reaches a maximum at the quantum-critical point, which is shifted due to the finite-size scaling to the right of γ_x^{cr} [40, 42]. The concurrence decays then to zero for higher γ_x values. As its peak indicates the quantum-critical transition [42, 68–71], we will use concurrence in presence of feedback for identifying the maximum of concurrence C_R^{max} with a precursor of the QPT in the thermodynamic limit. Indeed, the maximum of the concurrence for finite θ_x values is shifted with increasing θ_x values to the smaller γ_x , see red (dot-dashed) and green (solid) curves in the inset without additional markers. The curves marked with open (closed) symbols show the finite size effects for $N = 30(100)$. The critical point becomes then shifted by the feedback, too, as we have already observed in the previous section. The maximal concurrence C_R^{max} is shown in Fig. 6(left) along the blue solid line in Fig. 4 in the (γ_x, θ_x) plane. The blue dotted line shows the maximum concurrence for $N = 30$ particles. The finite-size shift is rather small, this suggests that the maximum of the concurrence is a more precise method to determine the final point of the dissipative QPT. The blue line can also be seen as the phase separation, left from the line the system is in the normal phase, right from it the system would be in the symmetry broken phase in the thermodynamic limit. Increasing the control parameter θ additionally shrinks the zone of the non-vanishing concurrence (colored zone in Fig. 6). Our numerics show that for $\theta \rightarrow \pi\sqrt{N}$ the zone with the normal phase vanishes. In this regime, the feedback action rotates the normal steady state immediately into a non-trivial one.

For completeness, the right part of Fig. 6 shows the concurrence for the J_z -control. The form of the contour plot mimics the behaviour of the $\langle J_z \rangle$ values from Fig. 4(right). With increasing θ_z , the area with non-vanishing concurrence shrinks and therefore the point of the dissipative QPT moves to the left. But for even larger values of θ_z , this trend is reversed and the QPT moves to the right again. At $\theta = \sqrt{N}\pi$ the old QPT without control is recovered as can be understood analytically from the spectrum of the J_z operator. Also here we observe that the maximum of concurrence is less sensitive to finite-size effects.

IV. SUMMARY

We have applied the Wiseman-Milburn control scheme to the dissipative Lipkin-Meshkov-Glick model by modifying the jump part of the corresponding master equation. The scheme monitors the reservoir and applies a kick in form of a unitary rotation around some spin axis

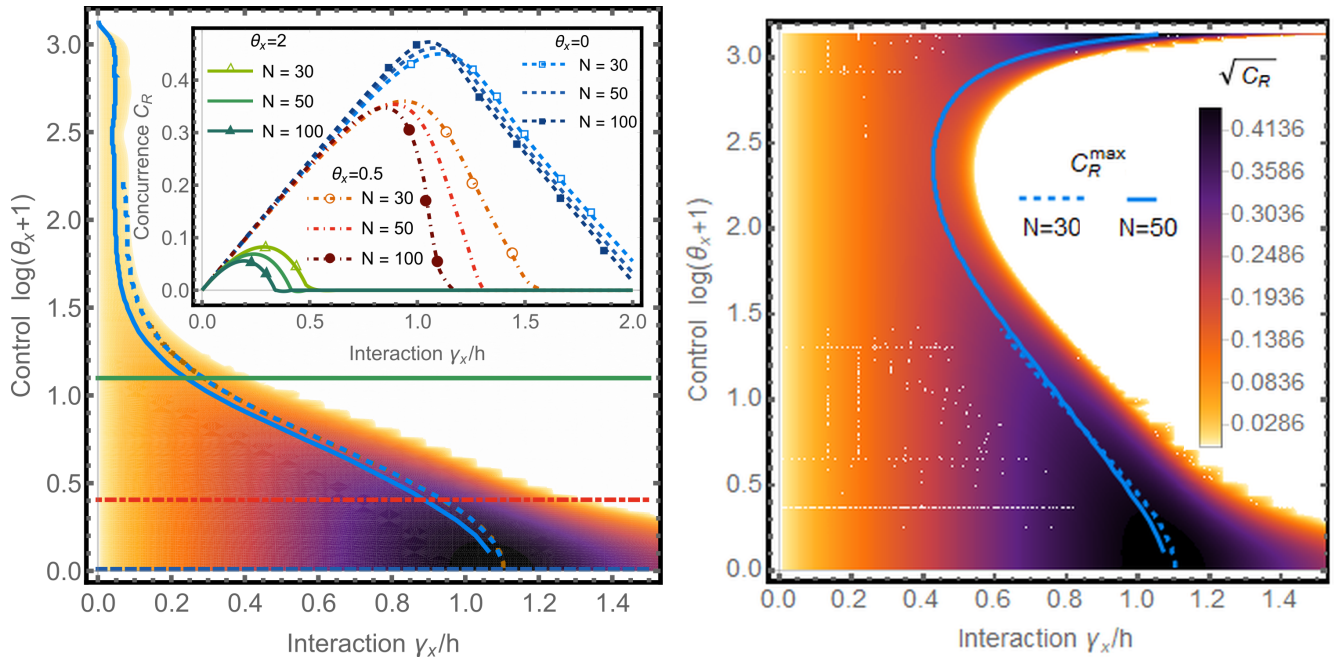


FIG. 6. Plot of the concurrence over the interaction γ_x and the control strength (note the logarithmic scaling) θ_x (left) or θ_z (right) for $N = 50$ and $\kappa = 0.05h$. The blue solid line marks the region with maximum concurrence C_R^{\max} and separates two phases of the LMG model in presence of feedback. The point with the maximal concurrence is shifted to smaller γ_x values and concurrence width shrinks with increasing control strength θ_x . In contrast, in presence of the J_z control (right) this trend is reversed for higher θ_z values. (Inset) The inset shows the concurrence shift for different θ_x values along the blue (dashed) [42], red (dot-dashed) and green (solid) horizontal cuts in the left contour plot. On top, we show the finite-size behaviour of the concurrence for different number of N , see lines marked with open ($N = 30$) and filled ($N = 100$) symbols.

after emission events. We determined numerically the steady state of the feedback master equation in the finite-size regime and used it to calculate the spin expectation values and the concurrence, which quantifies the spin-spin entanglement within the system. Without feedback, the $\langle J_z \rangle$ expectation value stays constant (up to finite-size corrections) while increasing the spin coupling γ_x , until the critical point γ_x^{cr} is reached, where the concurrence reaches there its maximum value. For $\gamma_x > \gamma_x^{\text{cr}}$ both observables start to decay. Our approach could reproduce these finite-size signatures of a dissipative quantum phase transition [13, 40, 42]. In presence of feedback, such signatures are shifted to smaller γ_x values and the shift can be controlled by the feedback parameter, which is a rotation angle around one of the three spin axis. The concurrence values becomes smaller and the region with non-zero concurrence shrinks by an active feedback loop. However, as is clear from its definition, the concurrence represents only a lower bound of entanglement which one could have in a system [41]. The applied feedback rotation cannot rotate the system into an eigenstate of the effective Hamiltonian since these would require significantly more sophisticated control operations. To implement general control operations would be highly non-trivial especially for larger N values. Therefore, we could detect the signatures of the intrinsic QPT in the spin expectation values as well. We believe that our meth-

ods can be useful in the study of other spin systems and feedback problems with delay as well.

ACKNOWLEDGEMENTS

We thank Javier Cerrillo for useful discussions. The authors gratefully acknowledge financial support from the DFG (grants BR 1528/9-1, SFB 910, GRK 1558).

APPENDIX

Using $\partial_t \langle J_\eta \rangle = \text{Tr}(J_\eta \dot{\rho})$ with the mean-field assumptions, the equations of motions without feedback become [18, 40]

$$\begin{aligned}
 X &= \frac{1}{j} \langle J_x \rangle, Y = \frac{1}{j} \langle J_y \rangle, Z = \frac{1}{j} \langle J_z \rangle \quad , \quad (\text{A.17}) \\
 \dot{X} &= hY - \frac{\kappa}{2} ZX, \\
 \dot{Y} &= -hX + \gamma_x ZX - \frac{\kappa}{2} ZY, \\
 \dot{Z} &= -\gamma_x XY + \frac{1}{2} (X^2 + Y^2).
 \end{aligned}$$

The equations from (A.17) have two steady-state solutions. The first one $(X, Y, Z) = (0, 0, 1)$ is stable in the

normal phase and the solution in (A.18) is stable for the symmetry-broken phase

$$\begin{aligned}
 A_{\pm} &= \kappa^2 \pm 4h^2, \quad B = \sqrt{\gamma_x^2 - \kappa^2}, \quad (\text{A.18}) \\
 X &= \pm \frac{1}{\sqrt{2\kappa}} \sqrt{A_- + \frac{1}{\gamma_x} B A_+}, \\
 Z &= \frac{2h}{\kappa^2} (\gamma_x - B), \\
 Y &= \frac{\kappa}{2h} XZ.
 \end{aligned}$$

The point where the stable solution changes denotes the point of the phase transition, it is given by Eq. (12) in the article.

-
- [1] H. Haken, Laser theory, Vol. xxv/2c of Encyclopedia of Physics (Berlin, 1970); reprint (Springer, 1984).
- [2] M. O. Scully, Quantum optics (Cambridge University Press, Cambridge, 1997).
- [3] P. C. Hohenberg and B. I. Halperin, *Rev. Mod. Phys.* **49**, 435 (1977).
- [4] S. Sachdev, Quantum phase transitions (Wiley Online Library, 2007).
- [5] R. H. Dicke, *Phys. Rev.* **93**, 99 (1954).
- [6] H. J. Lipkin, N. Meshkov, and A. Glick, *Nucl. Phys.* **62**, 188 (1965).
- [7] K. Hepp and E. H. Lieb, *Phys. Rev. A* **8**, 2517 (1973).
- [8] K. Hepp and E. H. Lieb, *Annals of Physics* **76**, 360 (1973).
- [9] L. M. Narducci, M. Orszag, and R. A. Tuft, *Phys. Rev. A* **8**, 1892 (1973).
- [10] Y. K. Wang and F. T. Hioe, *Phys. Rev. A* **7**, 831 (1973).
- [11] C. Emary and T. Brandes, *Phys. Rev. E* **67**, 066203 (2003).
- [12] P. Ribeiro, J. Vidal, and R. Mosseri, *Phys. Rev. Lett.* **99**, 050402 (2007).
- [13] S. Dusuel and J. Vidal, *Phys. Rev. Lett.* **93**, 237204 (2004).
- [14] D. Nagy, G. Szirmai, and P. Domokos, *Phys. Rev. A* **84**, 043637 (2011).
- [15] M. J. Bhaseen, J. Mayoh, B. D. Simons, and J. Keeling, *Phys. Rev. A* **85**, 013817 (2012).
- [16] W. Kopylov, C. Emary, and T. Brandes, *Phys. Rev. A* **87**, 043840 (2013).
- [17] T. E. Lee, C.-K. Chan, and S. F. Yelin, *Phys. Rev. A* **90**, 052109 (2014).
- [18] S. Morrison and A. S. Parkins, *Phys. Rev. Lett.* **100**, 040403 (2008).
- [19] M. Vogl, G. Schaller, and T. Brandes, *Phys. Rev. Lett.* **109**, 240402 (2012).
- [20] K. Baumann, C. Guerlin, F. Brennecke, and T. Esslinger, *Nature (London)* **464** (2010).
- [21] T. Zibold, E. Nicklas, C. Gross, and M. K. Oberthaler, *Phys. Rev. Lett.* **105**, 204101 (2010).
- [22] S. De Liberato, D. Gerace, I. Carusotto, and C. Ciuti, *Phys. Rev. A* **80**, 053810 (2009).
- [23] V. M. Bastidas, C. Emary, B. Regler, and T. Brandes, *Phys. Rev. Lett.* **108**, 043003 (2012).
- [24] O. Acevedo, L. Quiroga, F. Rodríguez, and N. Johnson, *New Journal of Physics* **17**, 093005 (2015).
- [25] W. Kopylov, C. Emary, E. Schöll, and T. Brandes, *New J. Phys.* **17**, 013040 (2015).
- [26] W. Kopylov, M. Radonjić, T. Brandes, A. Balaž, and A. Pelster, *Phys. Rev. A* **92**, 063832 (2015).
- [27] L. Droenner, N. L. Naumann, A. Knorr, and A. Carmele, arXiv:1801.03342 (2018).
- [28] F. M. Faulstich, M. Kraft, and A. Carmele, *Journal of Modern Optics*, 1 (2017).
- [29] J. Kabuss, D. O. Krimer, S. Rotter, K. Stannigel, A. Knorr, and A. Carmele, *Phys. Rev. A* **92**, 053801 (2015).
- [30] N. L. Naumann, S. M. Hein, M. Kraft, A. Knorr, and A. Carmele, “Feedback control of photon statistics,” (2017).
- [31] A. L. Grimsmo, *Phys. Rev. Lett.* **115**, 060402 (2015).
- [32] H. M. Wiseman and G. J. Milburn, Quantum measurement and control (Cambridge University Press, Cambridge, 2009).
- [33] H. M. Wiseman, *Phys. Rev. A* **49**, 2133 (1994).
- [34] J. Wang and H. M. Wiseman, *Phys. Rev. A* **64**, 063810 (2001).
- [35] C. Pörtl, C. Emary, and T. Brandes, *Phys. Rev. B* **84**, 085302 (2011).
- [36] G. Kießlich, C. Emary, G. Schaller, and T. Brandes, *New Journal of Physics* **14**, 123036 (2012).
- [37] D. Risté, C. C. Bultink, K. W. Lehnert, and L. DiCarlo, *Phys. Rev. Lett.* **109**, 240502 (2012).
- [38] P. Campagne-Ibarcq, E. Flurin, N. Roch, D. Darson, P. Morfin, M. Mirrahimi, M. H. Devoret, F. Mallet, and B. Huard, *Phys. Rev. X* **3**, 021008 (2013).
- [39] P. Strasberg, G. Schaller, T. Brandes, and M. Esposito, *Phys. Rev. E* **88**, 062107 (2013).
- [40] S. Morrison and A. S. Parkins, *Phys. Rev. A* **77**, 043810 (2008).
- [41] W. K. Wootters, *Phys. Rev. Lett.* **80**, 2245 (1998).
- [42] S. Dusuel and J. Vidal, *Phys. Rev. B* **71**, 224420 (2005).
- [43] R. Orús, S. Dusuel, and J. Vidal, *Phys. Rev. Lett.* **101**, 025701 (2008).
- [44] M. Caprio, P. Cejnar, and F. Iachello, *Annals of Physics* **323**, 1106 (2008).
- [45] S. Lerma-H and J. Dukelsky, *Journal of Physics: Conference Series* **492**, 012013 (2014).
- [46] W. Kopylov, G. Schaller, and T. Brandes, *Phys. Rev. E* **96**, 012153 (2017).
- [47] R. Gilmore and D. Feng, *Nuclear Physics A* **301**, 189 (1978).
- [48] R. Gilmore et al., *Physics Letters B* **76**, 26 (1978).
- [49] P. Ribeiro, J. Vidal, and R. Mosseri, *Phys. Rev. E* **78**, 021106 (2008).

- [50] P. Pérez-Fernández, A. Relaño, J. M. Arias, J. Dukelsky, and J. E. García-Ramos, *Phys. Rev. A* **80**, 032111 (2009).
- [51] T. Brandes, *Phys. Rev. E* **88**, 032133 (2013).
- [52] L. F. Santos and F. Pérez-Bernal, *Physical Review A* **92**, 050101 (2015).
- [53] P. Stránský, M. Macek, A. Leviatan, and P. Cejnar, *Annals of Physics* **356**, 57 (2015).
- [54] G. Engelhardt, V. M. Bastidas, W. Kopylov, and T. Brandes, *Phys. Rev. A* **91**, 013631 (2015).
- [55] P. Cejnar and P. Stránský, *Phys. Rev. E* **78**, 031130 (2008).
- [56] P. Cejnar and J. Jolie, *Progress in Particle and Nuclear Physics* **62**, 210 (2009).
- [57] H.-P. Breuer and F. Petruccione, The theory of open quantum systems (Oxford university press, 2002).
- [58] G. Schaller, Open Quantum Systems Far from Equilibrium (Springer, 2014).
- [59] C. Jung, M. Müller, and I. Rotter, *Phys. Rev. E* **60**, 114 (1999).
- [60] W. Kopylov and T. Brandes, *New Journal of Physics* **17**, 103031 (2015).
- [61] P. Solinas, P. Ribeiro, and R. Mosseri, *Phys. Rev. A* **78**, 052329 (2008).
- [62] C. H. Bennett, D. P. DiVincenzo, J. A. Smolin, and W. K. Wootters, *Phys. Rev. A* **54**, 3824 (1996).
- [63] J. I. Latorre, R. Orús, E. Rico, and J. Vidal, *Phys. Rev. A* **71**, 064101 (2005).
- [64] S. Hill and W. K. Wootters, *Phys. Rev. Lett.* **78**, 5022 (1997).
- [65] X. Wang and K. Mølmer, *The European Physical Journal D - Atomic, Molecular, Optical and Plasma Physics* **18**, 385 (2002).
- [66] S. Schneider and G. J. Milburn, *Phys. Rev. A* **65**, 042107 (2002).
- [67] J. Vidal, G. Palacios, and C. Aslangul, *Phys. Rev. A* **70**, 062304 (2004).
- [68] N. Lambert, C. Emary, and T. Brandes, *Phys. Rev. A* **71**, 053804 (2005).
- [69] S.-J. Gu, H.-Q. Lin, and Y.-Q. Li, *Phys. Rev. A* **68**, 042330 (2003).
- [70] S.-J. Gu, G.-S. Tian, and H.-Q. Lin, *New Journal of Physics* **8**, 61 (2006).
- [71] J. Vidal, G. Palacios, and R. Mosseri, *Phys. Rev. A* **69**, 022107 (2004).